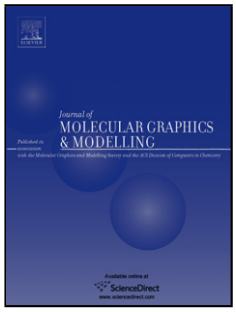

Title: DFT studies on *armchair* (5, 5) SWCNT functionalization. Modification of selected structural and spectroscopic parameters upon two-atom molecule attachment

Author: Marzena Nieradka Teobald Kupka Leszek Stobiński Jakub Kaminský

PII: S1093-3263(14)00183-1
DOI: http://dx.doi.org/doi:10.1016/j.jmgm.2014.11.006
Reference: JMG 6485

To appear in: *Journal of Molecular Graphics and Modelling*

Received date: 22-7-2014
Revised date: 19-9-2014
Accepted date: 7-11-2014

Please cite this article as: M. Nieradka, T. Kupka, L. Stobiński, J. Kaminský, DFT studies on *armchair* (5, 5) SWCNT functionalization. Modification of selected structural and spectroscopic parameters upon two-atom molecule attachment, *Journal of Molecular Graphics and Modelling* (2014), http://dx.doi.org/10.1016/j.jmgm.2014.11.006

Highlights

We model pristine armchair (5,5) single wall nanotube (SWCNT)

We model SWCNT- CO, NO, N2, H, and O2 adducts.

We examine changes in structural, IR/Raman and NMR parameters due to functionalization

Functionalization affects the DFT simulated IR/Raman and NMR spectra

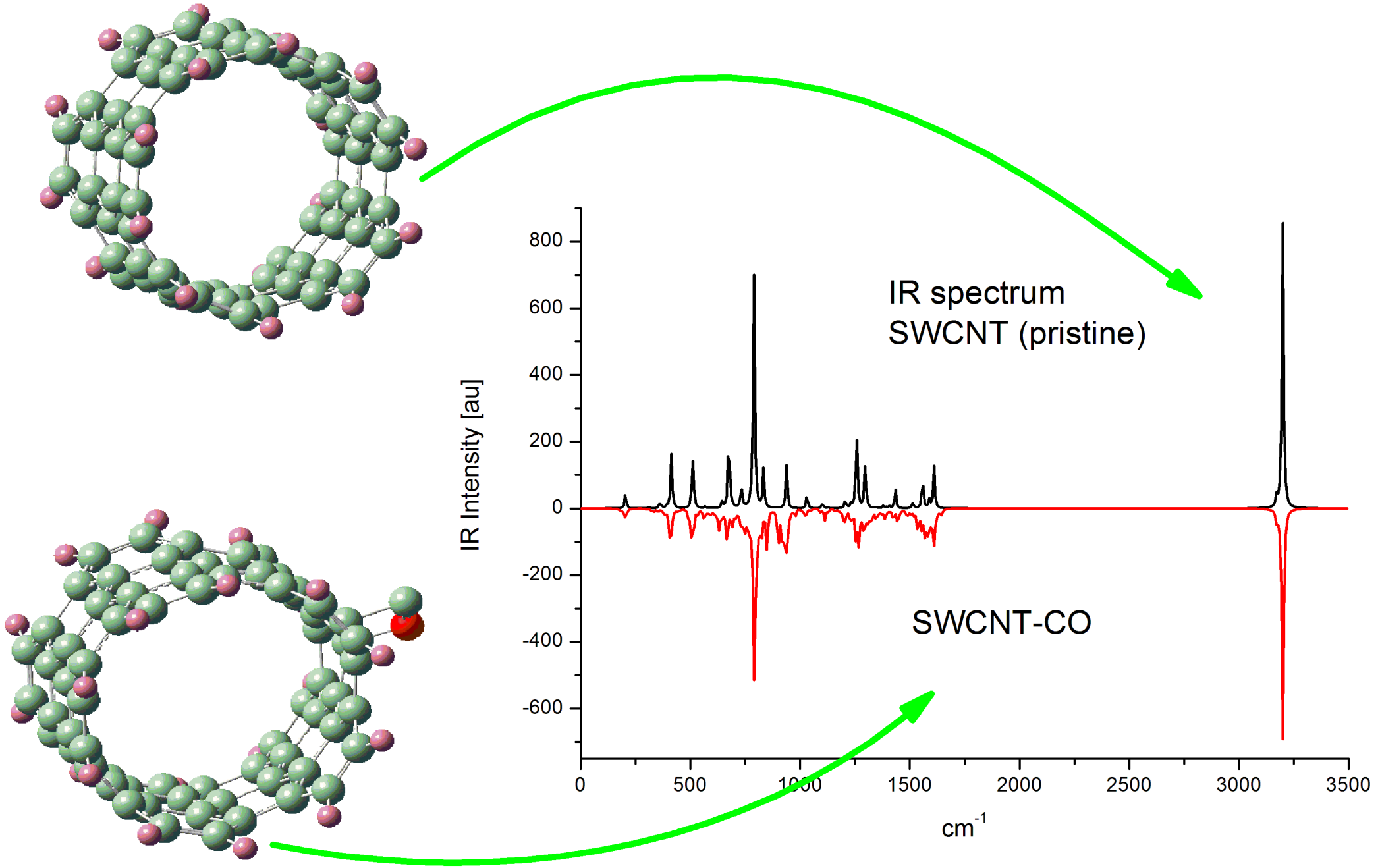
IR spectrum
SWCNT (pristine)
SWCNT-CO
IR Intensity [au]
800
600
400
200
0
-200
-400
-600
0
500
1000
1500
2000
2500
3000
3500
cm-1

Journal of Molecular Graphics and Modelling

DFT studies on *armchair* (5, 5) SWCNT functionalization. Modification of selected structural and spectroscopic parameters upon two-atom molecule attachment

Marzena Nieradka[1], Teobald Kupka[*,1], Leszek Stobiński[2] and Jakub Kaminský[*,3]

[1] University of Opole, Faculty of Chemistry, 48, Oleska Street, 45-052 Opole, Poland; [2] Institute of Physical Chemistry, Polish Academy of Sciences, 44/52, Kasprzaka, 01-224 Warsaw, Poland; [3]Institute of Organic Chemistry and Biochemistry, Czech Academy of Sciences, Flemingovo nám. 2., 166 10 Prague, Czech Republic

Abstract

Density functional theory (DFT) studies on adsorption of several gaseous homo- and hetero-diatomic molecules (AB) including H_2, O_2, N_2, NO and CO on external surface of H-capped pristine *armchair* (5, 5) single-walled carbon nanotube (SWCNT) were conducted. Structures of $C_{70}H_{10}$ and the corresponding $C_{70}H_{10}$–*AB* adducts were fully optimized at the B3LYP/6-311G* level of theory. Calculated HOMO/LUMO energy gaps (E_g), ^{13}C NMR chemical shifts and IR/Raman parameters were analyzed and critically compared with available experimental data. Significant changes of carbon NMR atom chemical shifts (up to –100 ppm) and shielding anisotropies (up to -180 ppm) at sites of addition were observed. Functionalized SWCNTs produced IR and Raman spectra different from the pristine nanotube model. The selective changes in vibrational spectra will help in assigning the topology of functionalization at the nanotube wall.

Keywords: single-walled carbon nanotube (SWCNT); absorption; *armchair*; DFT; NMR; HOMO/LUMO gap; IR; Raman

[*] *Correspondence to: Teobald Kupka, University of Opole, Faculty of Chemistry, 48, Oleska Street, 45-052 Opole, Poland: e-mail: teobaldk@gmail.com and Jakub Kaminsky, Institute of Organic Chemistry and Biochemistry, Czech Academy of Sciences, Prague, Czech Republic; e-mail: kaminsky@uochb.cas.cz*

1. Introduction

Since the last two decades, carbon nanotubes (CNTs) [1], fullerenes [2] and graphenes [3] have attracted enormous scientific and practical interest all over the world due to their exciting physical, optical, electronic, magnetic, and thermodynamic properties with potential applications in nanoelectronics, energy storage, chemical processes, biosensors, field emission displays and medical diagnostics and therapy [4-7].

Due to their high surface to volume ratio, the carbon nanotubes are suitable for adsorption of different gas molecules [8, 9]. The change in electronic and structural properties of carbon nanotubes and their exposure to environmental gases has been studied experimentally and theoretically. Thus, the CNTs were proposed as gas sensors [10-14]. An attachment of O_2**,** N_2, H_2, NO and CO molecules to external surface of *zigzag* SWCNT was modeled at the DFT level [15]. The authors observed significant changes of energetics and NMR parameters of potential applications to monitor the presence of these gases. Unfortunately, some interesting studies [8, 12-14] are not easy to follow. Their descriptions of molecular systems, calculations and results are unclear. Besides, these studies were not mentioned in the recent reports [16, 17]. Numerous studies reported also on heavy metal doped CNTs and their interactions with small molecules. All the studies concentrated on structural, electronic and energetic parameters of adsorption [18-20]. For example, the interactions between hydrogen, nitrogen, oxygen, nitrogen monoxide and carbon monoxide has significantly modified the intrinsic SWCNT electronic band gap [21, 22]. An interesting experimental (IR/Raman) and theoretical DFT studies on oxidation of carbon nanotubes appeared recently [23]. In 2000 Dai and coworkers [10] reported on an efficient NO_2 and NH_3 sensor, constructed from semi-conducting SWCNT. It is worth mentioning efficient gas sensing by these authors using SWCNTs at room-temperature measuring conditions.

Nuclear magnetic resonance (NMR) spectroscopy is among the most comprehensive techniques used in structural and electronic property studies of condensed-phase samples [24, 25]. The nuclear magnetic shielding tensor (σ_{ij}) traditionally experimentally expressed as chemical shift (δ_i in isotropic environment) and its anisotropy ($\Delta\sigma$) or individual components (σ_{ij}) for SWCNT samples are often extracted from solid state NMR spectra (in anisotropic environment) [26]. A demand for high precision calculations of NMR shieldings helping with detail interpretations of NMR spectra soon increased hand in hand with a development of computational techniques and hardware resources. NMR parameters of SWCNTs are commonly predicted using gauge including atomic orbitals (GIAO) NMR calculations [17, 27-32]. A study on pristine *armchair* (5, 5) SWCNT of 0.738 nm length [33] reported calculated (DFT) NMR parameters of *zigzag* SWCNTs and noticed significant changes of individual carbon shieldings as a result of CO, N_2 and O_2 adsorptions. Formation of SWCNT-*AB* products is formally treated as the addition of diatomic molecule *AB* on a SWCNT and a formation of two separate chemical bonds C-*A* and C-*B*. The partly delocalized C-C bond at the surface of SWCNT changes its character and forms a single bond. Studies only concentrated on final products from two separate substrates, e.g. SWCNT and a molecule of diatomics. The possible mechanism and conditions of chemical reaction (temperature, pressure, solvent, catalyst, etc.) leading to formation of SWCNT-*AB* has not been discussed. Such reaction resembles a formation of ethane from ethylene and dihydrogen as the simplest example [34]. Obviously, this is a reverse reaction:

$H_2C{=}CH_2 + H_2 \leftarrow\rightarrow H_3C{-}CH_3 + \text{Energy}$

In that sense, afore mentioned studies describe the final product of such hypothetical addition processes. From the practical point of view, similar reactions occur in many technological processes, e.g. hydrogenation and oxygenation reactions. The latter one is used

in cleaning of raw SWCNT material from amorphous carbon by boiling with concentrated acids and often leads to cutting off the more reactive tips of carbon nanotubes and functionalization of such formed rims (ends) with –OH, –COOH, C=O groups, peroxides or epoxides and introduction of structural defects.

It is possible to assume a theoretical formation of (5, 5) *armchair* and (9, 0) *zigzag* SWCNTs by cutting a popular C_{60} fullerene in the middle and adding subsequent belts formed by cyclacenes (see [35]) These metallic nanotubes are of roughly identical diameter (6.9 and 7.1 Å, as calculated at the B3LYP/3-21G level of theory [36, 37]. Interestingly, the energy of one hydrogen atom replacement at the rim of open end (9, 0) *zigzag* or (5, 5) armchair SWCNTs (with dangling bonds saturated with H atoms) by –OH or –COOH groups differed consistently (about -40 and -38 for hydroxylation and -21 and -16 kcal/mol for carboxylation of *zigzag* and *armchair* SWCNTs, see ref. [36, 37]. In the current study we selected *armchair* SWCNT for theoretical studies involving their interaction with several small molecules. However, due to a high number of time-consuming calculations, corresponding studies on *zigzag* SWCNTs will be a subject of next studies.

To our best knowledge, a systematic study of the impact of small molecule adsorption/addition on armchair SWCNT on the structural and spectroscopic features (e.g. NMR or IR/Raman) has not been reported. Note, the experimental NMR studies of SWCNTs are very demanding and solid-state measurements produce relatively broad signals as an average of different types of nanotubes presented in the sample. Besides, the presence of metal catalyst and amorphous carbon in a very inhomogeneous sample is an additional obstacle. A selective isotopic labeling of the produced SWCNTs in highly controlled conditions with ^{13}C labeling is possible, though not common [38]. In such cases, the NMR spectra show dominant peaks due to selected SWCNT sites with higher level of ^{13}C. On the other hand, significantly easier experimentally is to concentrate attention on small molecules

interacting or reacting with SWCNT. In that case, the NMR properties of small molecules in the gas phase (free) are completely different upon covalent binding with SWCNT. Note that weak interactions (van der Waals forces) are important in numerous systems where typical covalent bonds are not formed. Vibrational spectroscopy (IR/Raman) is a typical mean for identification of carbon nanotubes [39]. In particular, the position of Raman breathing mode (RBM) at 200-300cm^{-1} in spectra of single-walled carbon nanotubes allowed to determine the tube diameter [39]. Another characteristic vibrational features occurring in carbon nanomaterials are D band (~1300 cm^{-1}, originating from structural defects), G band (~1600 cm^{-1}, set of tangential vibrations) and G' band (~2700 cm^{-1}, second overtone of the D band). Other overtones (e.g. G+RBM) are also frequently presented in Raman spectra, but they are of less importance. The G/D band intensity ratio can be used to derive information about purity of carbon nanomaterials [40].

Functionalization of SWCNT walls (sides) at different points (sites) is important for production of potentially soluble and better interacting nanotubes with polymer matrix during formation of novel composite materials. However, for a more efficient control of an industrial process it is important to know the localisation of specific substitution sites. Unfortunately, the knowledge about topology of substitution sites cannot be visualized using experimental imaging techniques (e.g. TEM, SEM or XRD [41]). We hope that this issue could be partly addressed by vibrational spectroscopy (IR/Raman) combined with molecular modelling. The aim of this paper is to report on the sensitivity of NMR, IR and Raman parameters upon hypothetical addition of small diatomics gas molecules to the surface of finite model of *armchair* SWCNT. The changes of parameters in an *armchair* (5, 5) SWCNT composed of 5 units (or belts formed by carbon hexagons) and interacting with O_2**,** N_2, H_2, NO and CO will be modeled using the DFT level of theory and compared with available theoretical results. Subtle changes of NMR parameters or vibrational features of SWCNTs

upon the addition of diatomic molecules will be critically analyzed. The mechanism of such functionalization, reactivity and kinetics is out of scope of this work.

2. Computational methods

All calculations on finite models of *armchair* SWCNTs and small molecules were performed with Gaussian 09 [42]. The pristine *armchair* (5, 5) SWCNT of 0.702 nm diameter and tube length of 0.731 nm was formed from twenty five fused hexagonal carbon rings, capped with hydrogen atoms at both ends (see Figure 1). The pristine SWCNT structure was fully optimized in the gas phase at the B3LYP/6-311G* level of theory.

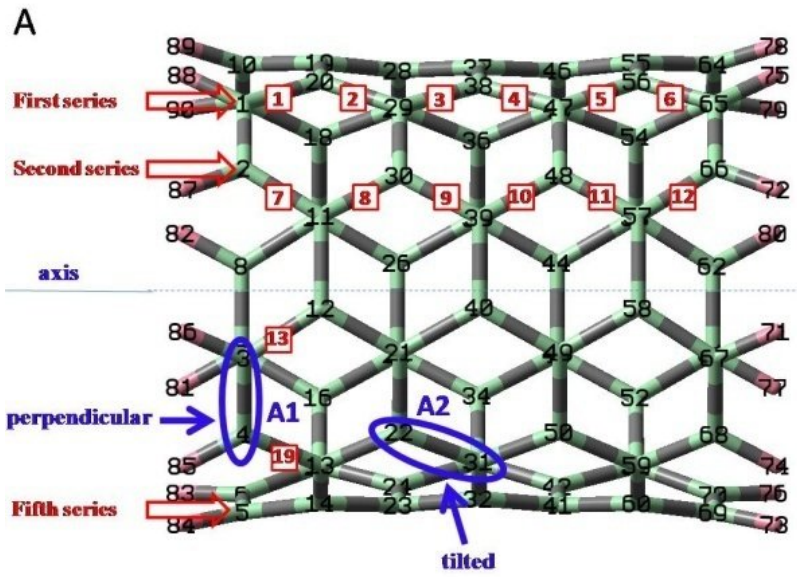

Figure 1. The B3LYP/6-31G* optimized model of *armchair* (5, 5) SWCNT. A1 and A2 adsorption sites including C3, C4 and C22, C31 carbons are marked in blue. Two types of C-C bonds, tilted and perpendicular are marked off, too.

Five small diatomic molecules were arbitrary selected as potential covalent adducts: H_2, O_2, N_2, CO and NO [18-20]. Subsequently, the optimization of *armchair* (5, 5) SWCNT together with diatomic adducts at C3, C4 (position A1, see Figure 1) or C22, C31 (position A2) was performed. A vibrational analysis at the same level of theory was performed to assure energy minimum of the modelled structures. The addition (or chemical adsorption) energy (E_{ad} in kcal/mol) of the studied molecules AB by a finite model of SWCNT was calculated as follows:

$$E_{ad} = E(SWCNT \cdots AB) - E(SWCNT) - E(AB) \quad (1)$$

where AB = H_2, N_2, O_2, CO, NO and E(SWCNT$\cdots AB$), E(SWCNT) and $E(AB)$ are the corresponding energies of the optimized adduct, nanotube and the covalently adsorbed molecule, respectively.

The GIAO NMR [17, 27-32] calculations on previously optimized structures were performed using the CAM-B3LYP/STO-3G$_{mag}$ level of theory [43, 44]. The CAM-B3LYP [43] density functional was recently used for accurate prediction of ^{13}C NMR shieldings in fullerenes [45] and van der Waals dimers [46]. The modified STO-3G basis set was recently introduced [44] as an efficient alternative for accurate calculations of carbon nuclear magnetic shieldings. Its excellent performance was recently confirmed.[47-49] The nuclear magnetic shielding tensor σ_{ij} (in ppm) of i-th nucleus [29, 50, 51] was calculated as a second derivative of the total energy (E) with respect to nuclear moment (μ_i) and magnetic field (B_j): $\sigma_{ij} = \partial^2 E / \left(\partial \mu_i \partial B_j\right)_{\mu_i B_j = 0}$. The isotropic nuclear magnetic shielding of i-th nucleus (in ppm) was calculated as an average of the shielding components: $\sigma_{iso} = (\sigma_{xx} + \sigma_{yy} + \sigma_{zz})/3$. The shielding anisotropy $\Delta\sigma^{(n)}$ (in ppm), for $\sigma_{zz}>\sigma_{yy}>\sigma_{xx}$, was calculated as follows: $\Delta\sigma^{(n)} = \sigma_{zz} - (\sigma_{xx} + \sigma_{yy})/2$ and the asymmetry parameter η was calculated as $\eta = 3(\sigma_{22} + \sigma_{11})/2\Delta\sigma$. The isotropic nuclear shielding is usually converted to chemical shift (in ppm) in experimental spectra using a reference molecule: $\delta_i = \sigma_0 - \sigma_i$. Tetramethylsilane, benzene, water and nitromethane were used as reference molecules (calculated at the same level of theory) [28, 29, 32, 52]. Benzene was used as the secondary reference better compensating the systematic errors [52, 53]. The B3LYP/6-311G* calculated IR/Raman spectra of pristine SWCNT and the corresponding diatomic adducts were processed in GaussView [54].

3. Results

3.1. Structure of pristine armchair (5, 5) SWCNT.

Two general kinds of CC bonds forming the nanotube and their arbitrary labeling are shown schematically in Figures 2A and B. Note, the optimized structure of pristine *armchair* (5, 5) SWCNT is highly symmetrical (see Figure 1). This is also apparent from Figure 3A showing a distribution of individual CC bonds perpendicular to the tube axis (around the tube surface).

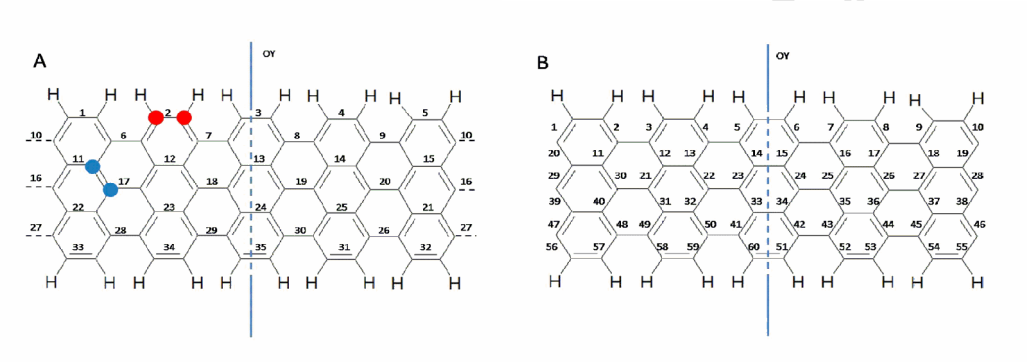

Figure 2. Different kinds of CC bonds in *armchair* (5, 5) SWCNT and their labeling are divided into (A) perpendicular and (B) tilted starting from one nanotube site to the opposite end. Adsorption sites (atoms C3, C4 and C22, C31) are marked as red (A1) and blue (A2) spots

There are seven series of horizontal CC bonds (perpendicular to the tube axis) in our *armchair* (5, 5) SWCNT and each of them consists of five identical CC bonds (e.g., bond No. 1 to 5 in the first series, see Figure 2A). The perpendicular CC bonds are symmetrically distributed along the axis with respect to the middle of the tube (e. g., series No. 1 = series No. 7, series No. 2 = series No. 6 and series No. 3 = series No. 5). Interestingly, the shortest bonds are at the rim (CC lengths in series No. 1 and 7 are 1.37 Å) while the longest bonds are in consecutive layers (CC bond lengths in series No. 2 and 6 are 1.45 Å). Thus, the

magnitudes of CC bonds at the rim are close to a typical double C=C bond (1.33 Å) but the longest ones are still about 0.1 Å shorter than the typical single CC bond (1.54 Å).

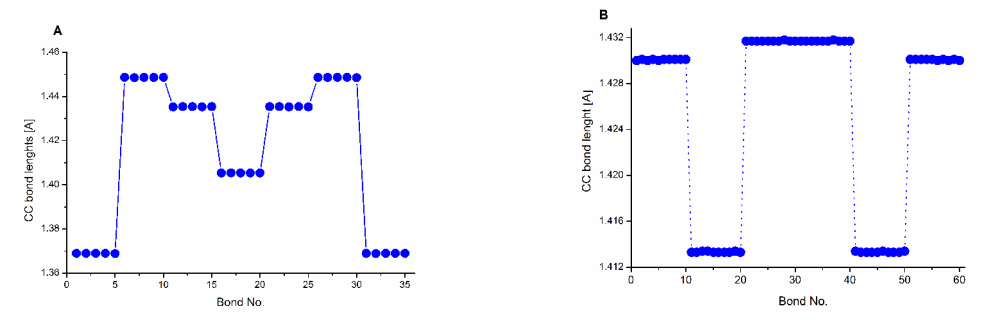

Figure 3. Distribution of CC bond lengths in separate series of bonds (A) around the *armchair* (5, 5) surface (perpendicular to the axis) and (B) along the nanotube (tilted).

A different picture is apparent from Figure 3B. In this case the CC bonds (labeled from 20 to 40) are viewed along the nanotube axis and the longest bonds (1.43 Å) are at the middle of the tube length. The shortest CC bonds (1.41 Å) appear closer to the tube ends. Note, the changes of CC bond lengths along the axis are significantly smaller (from 1.41 to 1.43 Å) than for the bonds perpendicular to the axis (from 1.37 to 1.45 Å).

3.2. Structure of armchair (5, 5) SWCNT with covalently bonded diatomics.

The bond character in the diatomic molecules can change as a result of their elongation, change of bond order (e. g. a decrease from double to single, or from triple to double bond) or their breaking upon covalent bonding with SWCNT surface. Selected types of experimental bond lengths are shown in Table S1 (for brevity placed in the supplementary material) and the interatomic distances in free and covalently bonded diatomic are gathered in Table S2. The first big change is for H…H distance (1.8 Å) indicating a complete breaking of bond comparing to the free dihydrogen (0.74 Å). In the remaining cases only a decrease of bond order is observed. For example, the triple bond in N_2 changes to a double one (see Table 1).

Addition of diatomics should also change the structure of the pristine SWCNT scaffold itself. In the first case we will analyze the impact of H_2 attachment to position A1 on the CC bond length changes in bonds perpendicular to the nanotube axis (Figure 4A) and along the axis (Figure 4B). A significant increase of CC bond length (about 0.18 Å) upon the addition is apparent from the Figure 4A. The next series of CC bonds experience a significantly smaller change (a decrease by about 0.03 Å). However, the last series (seventh) also experiences some subtle change (CC bonds elongated by 0.003 Å). The relative changes of CC bond lengths along the nanotube axis upon H_2 addition to position A1 are shown in the Figure 4B. A fairly large increase of CC bond lengths (about 0.09 Å) upon addition of H_2 is apparent (about two times smaller than in Figure 4A). However, comparing the tilted bonds with the corresponding ones in a free SWCNT, the pattern here is more scattered along the whole nanotube.

Table 1. Change of interatomic distances [in Å] in diatomics from free to bound state. Experimental values are given for a comparison.

AB	**Free**		**SWCNT-AB**		**Change of bondtype**
	Exp.	**Calc.**	**Δ A1**	**Δ A2**	
H-H	0.741[a]	0.742	1.622	1.515	breaking
N≡N	1.098[a]	1.148	0.109	0.107	triple to double
O=O	1.208[a]	1.207	0.281	0.286	double to single
C≡O	1.128[a]	1.127	0.199	0.194	triple to *quasi* double
N=O	1.22[b]	1.095	0.300	0.376	triple to double

a) From ref.[55]; b) From ref.[56]

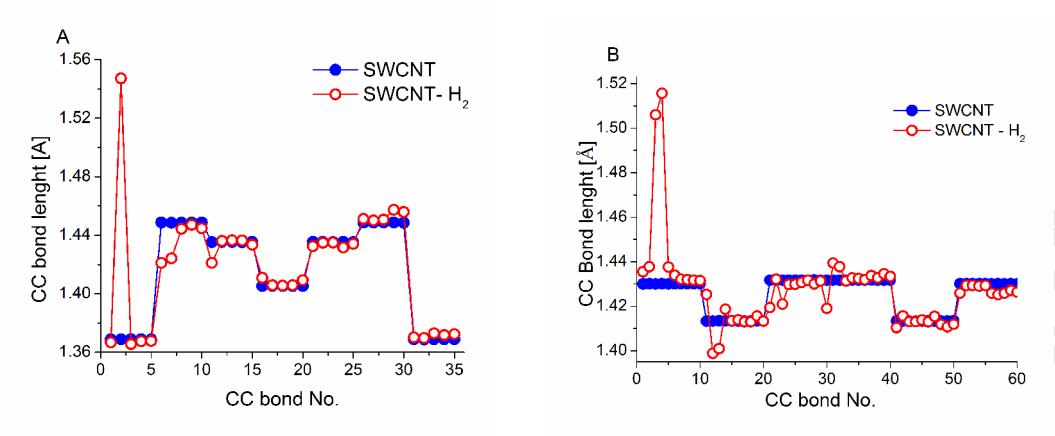

Figure 4. Distribution of CC bond lengths for pristine *armchair* (5, 5) SWCNT (blue marks) and with covalently bonded H_2 in position A1 (red open circles): (A) perpendicular to the nanotube axis and (B) tilted with respect to the nanotube axis.

On the other hand, addition of H_2 to position A2 distorts the SWCNT structure more and results in a significantly more complex pattern of CC bond changes, both perpendicular to the tube axis (Figure 5A) and tilted to the nanotube axis (Figure 5B). The magnitude of the observed CC bond increase (and decrease) in Figure 5A is smaller than in Figure 4A (0.10 – 0.12 Å and -0.07 vs. 0.18 Å) and slightly larger in the Figure 5B (0.12 Å vs. 0.1 A in the Figure 4B). The observed magnitudes of CC bond lengths in Figures 4 and 5 by 0.1 to 0.2 Å indicate the decreased CC bond order (see Table 1).

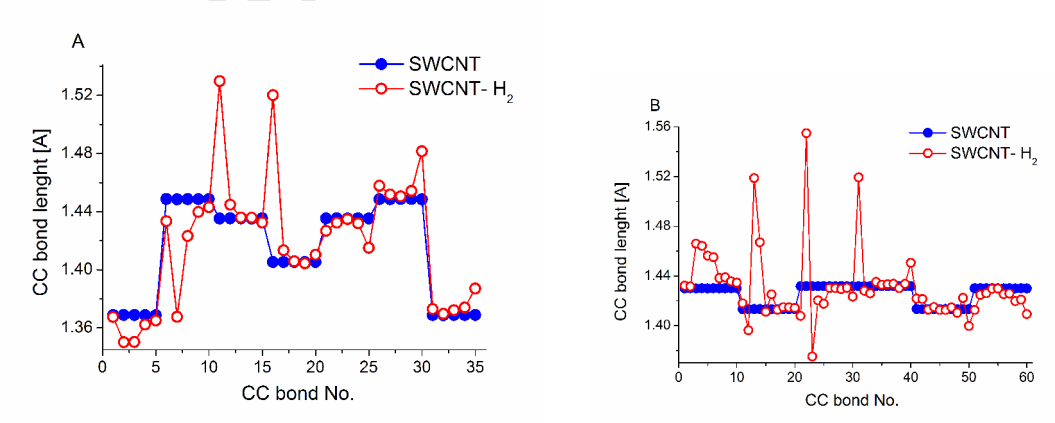

Figure 5. Distribution of CC bond lengths for pristine *armchair* (5, 5) SWCNT (blue marks) and with covalently bonded H_2 in position A2 (red open circles): (A) perpendicular to the nanotube axis and (B) tilted with respect to the nanotube axis

The changes of CC bonds introduced by addition of N_2, O_2, NO and CO molecules to *armchair* (5, 5) SWCNT were qualitatively identical to those, caused by H_2. Thus, for brevity the graphical presentations, similar to those in Figures 4 and 5 are included in the supplementary material (Figures S1A-S1B). Addition of diatomics to the position A1 causes the largest increase of perpendicular CC bonds in case of N_2 (0.22 Å) and slightly smaller for other molecules (CO by 0.20 Å, NO by 0.19 Å and O_2 by 0.18 Å). The largest increases of CC tilted bonds are for H_2 (0.08 Å) and slightly smaller for N_2, NO, CO and O_2 (0.06 Å).

Addition of diatomics to A2 follows the trend of addition to A1. The biggest increase of perpendicular CC bonds is for N_2 (0.14 Å) and slightly smaller for other molecules (CO and H_2 by 0.12 Å, O_2 by 0.11 Å and NO by 0.09 Å). The largest increases of tilted CC bonds are for H_2 (0.12 Å) and slightly smaller for O_2 (0.11 Å), N_2 and CO (0.10 Å) and NO (0.09 Å) (Figures S2A-S2B).

3.3. Electronic properties of SWCNT-AB adducts.

All the SWCNT-*AB* adducts were fully optimized and structures were proved as energy minima. Note, the formation of such adducts possibly involves an *AB* bond breaking or decreasing its bond order. Thus, our final products can in fact be only intermediates, but reaction mechanism study is beyond the scope of this work. However, we believe the general conclusion made here will hold for real SWCNT-*AB* product too. Finally, changing of one aromatic C=C bond into a single C-C bond and formation of two new single bonds (C-A and C-B) accompany the addition of diatomics on the SWCNT surface.

The energy needed for a hypothetic and simplified addition reaction (e.g. an oxygenation of SWCNT) is supplied during the reaction. For example, in the process of raw

material cleaning comes from heating it with a mixture of concentrated acids, and $KMnO_4$ as oxidizer. This value includes all the formal terms, responsible for breaking and/or forming new bonds. Due to a low level of theory (adjusted to the studied system size) the obtained values of energy are of semi quantitative nature and are more appropriate as indicators of general trends. For this reason, the energy of addition will not be discussed in the current study.

The electronic properties of pristine and functionalized SWCNTs are often characterized in terms of their HOMO and LUMO energies and the corresponding energy gap (E_g in eV), which is often an indicator for characterization of SWCNT as metallic, semiconductors or insulators (near zero, around 1 and above 6 eV, respectively). There is a very good agreement between published DFT values of HOMO, LUMO and E_g for the pristine SWCNT and our results (see Table 2). Thus, we are confident about our remaining results for the SWCNT-*AB* systems (adducts at the positions A1 and A2).

Table 2. The B3LYP calculated HOMO, LUMO and E_g energies (in eV) for adducts at A1 and A2 positions.

	E_{HOMO}	E_{LUMO}	E_g
SWCNT	-4.810	-2.6419	2.1682
	A1		
SWCNT-H_2	-4.671	-2.689	1.982
SWCNT-N_2	-4.880	-2.907	1.974
SWCNT-O_2	-4.882	-2.936	1.946
SWCNT-CO	-4.890	-2.918	1.972
SWCNT-NO	-4.867	-2.926	1.941
	A2		
SWCNT-H_2	-4.648	-2.765	1.883
SWCNT-N_2	-4.836	-3.062	1.774
SWCNT-O_2	-4.867	-3.089	1.778
SWCNT-CO	-4.908	-3.126	1.781
SWCNT-NO	-4.794	-2.660	2.134

In the case of H_2, the HOMO of SWCNT-H_2 adduct is higher by about 0.15 eV than for the pristine SWCNT (and LUMO decreases by ~0.05 eV). Contrary to SWCNT-H_2, all other adducts produce HOMO and LUMO lower in energy than has original pristine SWCNT. The E_g changes from 2.17 (in SWCNT) to even 1.77 eV (in SWCNT-N_2). The E_g values for most adducts are slightly smaller than for H_2. According to results the reaction product (adduct) is less stable and more reactive (E_g of SWCNT-*AB* < E_g of SWCNT) than for original SWCNT. Note that the reaction energy (*E* of addition) is negative, so the process is exothermic. The results gathered in the Table 2 thus suggest a significant change of electronic properties of initial pristine *armchair* (5, 5) SWCNT upon chemical (covalent) bonding of the selected diatomics. Figure 6 shows a spatial arrangement and localization of HOMO and LUMO orbitals on the standard *armchair* (5, 5) SWCNT and H_2-adduct. It is visible that HOMO is localized over the CC bond going more or less along the tube axis and is at the rim of the tube. LUMO is localized on carbon atoms defining the same bond. Note, that both HOMO and LUMO are highly degenerated and thus there is a certain number of HOMO-*N* or LUMO+*N* with similar spatial and energy characteristics, which are spread over the whole SWCNT cage. Perturbation introduced by H_2 at the position A1 evoked different ordering of degenerated orbitals and thus HOMO and LUMO are spatially shifted to different CC bond.

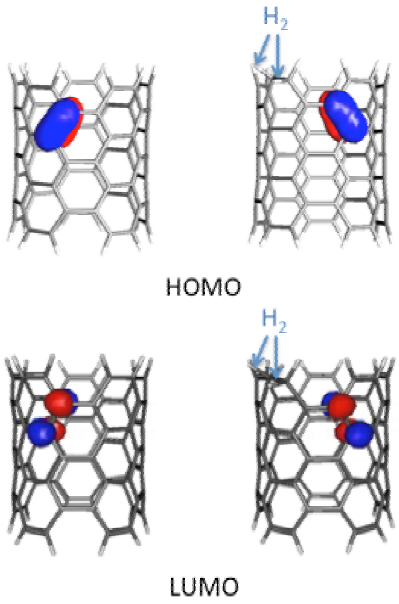

Figure 6. HOMO-LUMO plots for *armchair* (5, 5) SWCNT (left panels) and (5, 5) SWCNT-H_2 adduct (right panels).

3.4. Monitoring the SWCNT-AB formation by NMR.

NMR parameters of free and covalently attached diatomics to SWCNT will differ due to variations in local electronic (and magnetic) environment. Thus, it will be easier to observe experimentally diatomics than the carbon nanotube sample. In such case a typical high resolution NMR spectrometer should be used, in particular when we use isotopically labeled gases (^{2}H and ^{13}C are readily available, ^{15}N or ^{17}O are more expensive). Therefore, in the first step we concentrate on changes in isotropic shieldings of diatomics upon their incorporation into the *armchair* (5, 5) SWCNT structure (Table 3). It is apparent that in case of dihydrogen the changes are relatively small (less than 1 ppm). Significantly larger changes are predicted for N_2 (ca. -340). Similarly, the O_2 addition leads to a change of the corresponding ^{17}O signal, which is one order of magnitude smaller than for ^{15}N shieldings in N_2 adducts. Incorporation of carbon monoxide could be successfully monitored by changes of either ^{13}C isotropic shielding (Δ of about -300 ppm) or ^{17}O shielding (Δ of about -140 ppm).

Table 3. Changes of isotropic nuclear magnetic shieldings (σ_{iso}, in ppm) of free and bonded diatomics ($\Delta\sigma$ = (SWCNT-*AB*) – (*AB),* where *AB* = H_2, N_2, O_2 and CO, in ppm) at certain position.

Carbon	^{1}H (H_2)	^{15}N (N_2)	^{17}O (O_2)	^{13}C (CO)	^{17}O (CO)
			σ_{iso}(free gas)		
	27.09	-110.64	-74.40	-38.10	-103.63
			$\Delta(\sigma_{iso,}$adducts)		
C3	0.91	-341.70	63.07	-312.64	
C4	0.74	-341.72	63.09		-142.53
C22	0.71	-353.84	23.33	-299.09	
C31	0.16	-338.55	29.44		-137.23

As the next step we will assess changes of ^{13}C NMR parameters for individual carbon atoms in the model SWCNT upon addition of diatomics. The B3LYP shielding tensor components (σ_{ii}), isotropic values, anisotropies ($\Delta\sigma$) and asymmetry parameters (η) for selected carbon atoms in *armchair* (5, 5) SWCNT before and after addition of diatomics are gathered in Table 4. These parameters are readily observed in solid-state ^{13}C NMR spectra and better reflect the local electronic environment of a nuclear spin within a molecular fragment than the results of an experiment in solution, for which only one NMR parameter is available (the isotropic value).

In all cases there are significant modifications of ^{13}C parameters upon addition of diatomics. Changes are observed for shielding anisotropy (about 2 – 150 ppm) and shielding tensor components (from 30 to 300 ppm). In contrary, smaller changes of isotropic shielding values are predicted (from about 2 to 100 ppm). Having six different NMR parameters for every selected carbon atom in hand, this should help to distinguish between individual position additions (in our case A1 and A2).

The crucial for reliable predictions is to assess the accuracy of calculated NMR parameters. Theoretical (B3LYP/STO-3G$_{mag}$) ^{13}C chemical shifts in *armchair* (5, 5) SWCNT

and available solution-phase experimental results of chiral (6, 5) SWCNT are compared [38] in Figure 7. Despite a very simplified theoretical model, a very good agreement between the chemical shift of carbons in the middle of the model *armchair* nanotube (~128 ppm) and the experiment (~129 ppm) is apparent, which agree well with the idea of real-size nanotube with large number of such "internal" carbons. We would like to notice that recent solid-state NMR experiments on chiral (6, 5) SWCNTs showed a single ^{13}C signal at 129 ppm [38] as well.

Results presented in Table 4 and Figures 7 clearly indicate a reasonable sensitivity of NMR technique to addition of small-size diatomics to *armchair* nanotubes.

Table 4. CAM-B3LYP calculated shielding tensor components (σ_{ii}, in ppm), its isotropic value (σ_{iso}, in ppm), anisotropy ($\Delta\sigma$, in ppm) and asymmetry parameter (η) for the selected carbon atoms in *armchair* (5, 5) SWCNT upon addition of diatomics

	Carbon	Tensor components			σ_{iso}	$\Delta\sigma$	η
		σ_{11}	σ_{22}	σ_{33}			
SWCNT	C3	-55.12	32.71	167.21	48.27	178.42	0.74
	C4	-55.11	32.68	167.21	48.26	178.43	0.74
	C22	-39.27	-5.07	177.13	44.32	199.23	0.26
	C31	-32.43	-8.73	173.38	44.07	193.95	0.18
SWCNT-H_2	C3	142.79	153.88	165.50	154.06	17.16	0.97
	C4	127.96	152.58	156.82	145.79	16.55	2.23
	C22	133.01	142.59	148.85	141.48	11.05	1.30
	C31	132.80	144.82	147.94	141.86	9.13	1.97
SWCNT-O_2	C3	64.41	80.82	147.02	97.42	74.40	0.33
	C4	64.42	80.79	147.01	97.41	74.41	0.33
	C22	-63.38	50.40	153.40	90.10	159.89	1.07
	C31	-61.47	45.86	154.18	91.90	161.98	0.99
SWCNT-N_2	C3	57.21	89.24	131.03	92.50	57.81	0.83
	C4	57.24	89.26	131.04	92.51	57.80	0.83
	C22	61.55	80.14	128.32	90.00	57.48	0.48
	C31	59.82	79.23	122.70	87.25	53.18	0.55
SWCNT-CO	C3	30.78	68.61	138.41	79.27	88.72	0.64
	C4	57.38	122.50	143.79	107.89	53.85	1.81
	C22	-81.86	43.62	156.73	141.23	175.85	1.07
	C31	-60.59	59.63	156.45	52.68	156.93	1.15
SWCNT-NO	C3	51.42	75.07	140.76	89.08	77.51	0.46
	C4	73.04	104.64	138.46	105.38	49.62	0.95
	C22	65.68	81.66	141.41	96.25	67.74	0.35
	C31	86.44	111.45	144.91	114.27	45.97	0.82

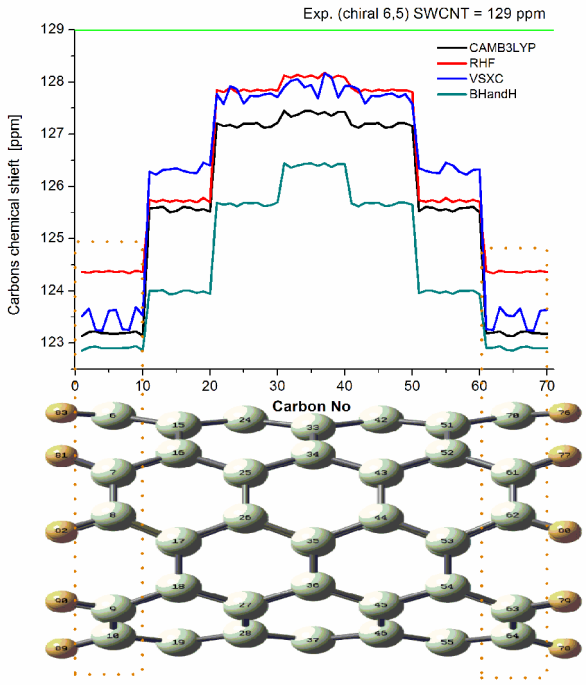

Figure 7. Distribution of individual carbon chemical shifts along the axis of *armchair* (5, 5) SWCNT. Experimental value for chiral (6,5) SWCNT [38] is plotted (continuous green line) for comparison.

3.5. Monitoring the SWCNT-AB formation by IR and Raman spectroscopy.

In Figures 8-9 there are B3LYP/6-311G* calculated Raman spectra of the pristine and functionalized *armchair* (5, 5) SWCNTs. Corresponding IR spectra are in SI. The spectral intensities are normalized with respect to intense ν(CH) signal. Its intensity and position was practically unchanged upon substitution with *AB* molecules. We would like to notice that hydrogen vibrations at the rim strongly mix with the motion of the carbon skeleton, and thus their "artificial presence" in our models comparing to real nanotubes calculated spectra provide only a qualitative picture. This is mostly the case of longitudinal optical phonon mode. It is apparent from the spectra in Figure 8 that contrary to IR results (Figure S4), there

is a significantly smaller number of Raman active vibrations for pristine SWCNT. Problems with hydrogen interfering CC vibrations can be seen especially in low-intensity bands at 1199, 1226 or 1275 cm^{-1} corresponding to CC stretching (along or perpendicular to the tube axis) coupled with CCH bending vibrations. The overlap of CCH bending vibration region with the CC stretching region can be clearly seen from the potential energy distribution (PED) of SWCNT internal coordinates in Figure 9. The PED within the harmonic approximation enables a convenient assignment of molecular vibrational motions to local coordinates [57, 58]. It is usually difficult to manually define a non-redundant set of coordinates for the whole molecule, thus a computer program was used for the (5, 5) SWCNT, in order to automatically define a redundant set of internal coordinates comprising all stretchings, bendings and torsion angles based on the covalent bond pattern as shown before [59]. The unrealistically intense Raman signal due to C=C stretch was observed near 1350 cm^{-1}. It is difficult to state, whether this band is strictly affected by hydrogens and thus can be attributed to a disorder induced D-modes[60]. Smaller (its intensity is roughly four times lower than the band at 1350 cm^{-1}) appears at about 1538 cm^{-1} or even les intensive band at 1611 cm^{-1}. Those bands most likely correspond to G-band tangential vibrations covering both symmetric and asymmetric CC vibrations along the tube axis or the circumference. Note also that the intensity ratios of bands at 1350 and 1538 cm^{-1} can change due to several factors (tube length or width). Moreover, the curvature effect might shift the peak positions of the G-band as well as other bands.

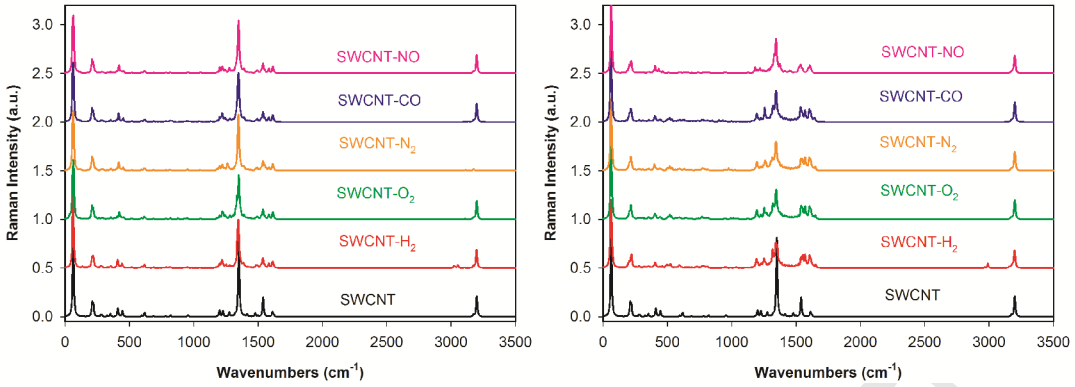

Figure 8. The B3LYP/6-311G* calculated Raman spectra of free *armchair* (5, 5) SWCNT and the studied SWCNT-*AB* adducts at position A1 (left) and position A2 (right).

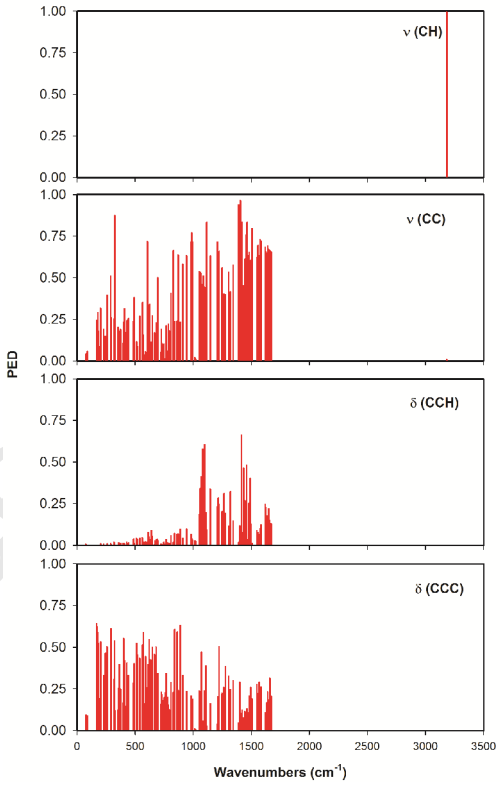

Figure 9. Calculated (B3LYP/6-311G**) relative potential energy distribution (PED) of internal coordinates of *armchair* (5, 5) SWCNT. Only contributions of ν(CH) and ν(CC) stretching and δ(CCH) and δ(CCC) bending modes are displayed.

4. Discussion

4.1. Rim or central position discrimination

Results presented in this paper can be seen from two different perspectives. One considers addition of diatomic molecules on the SWCNT at CC bonds that are perpendicular or parallel with the tube axes. However, for practical reasons and future applications seems to be whether the diatomic sits at the rim or it is attached in central part of the tube.

Analyzing the data from Table 2 it is obvious that the change of HOMO energetics upon the addition of diatomics to SWCNT is uniform for an attachment at the rim and in central part of SWCNT. Slightly larger difference can be observed for LUMO energies, where addition in the middle of the tube caused slightly larger increase of E_{LUMO} (average Δ of -0.34 eV, relative to pristine SWCNT) than it is at the rim addition (Δ of -0.28 eV). The difference between positions is even more pronounced in the E_g value, where the attachment of a diatomic at the rim caused a decrease of about 0.21 eV (relative to pristine value; average for all diatomics), while the addition in the middle of the tube decreases E_g of about 0.30 eV. Tubes modified in their central part are regarding their smaller E_g slightly more reactive comparing to those modified at the rim.

It is obvious from Table 3 we can probe the position of an attached diatomic also using heteronuclear NMR. Especially ^{17}O seems to be a very sensitive probe. The $\Delta\sigma_{iso}$ of ^{17}O is almost three-times higher when the O_2 sits at the rim than when it is in the central part of the tube. Considering the NMR signals of carbon atoms of the tube, we found out that the chemical shift difference between carbons at the rim and in the middle of the model (6, 5) SWCNT tube is only about 4.5 ppm. In our previous work [61] on *zigzag* (n, 0) SWCNTs we observed a large difference between chemical shift of carbons at the rim and the adjacent ones

(35 ppm for (6, 0) SWCNT and 20 ppm for (9, 0) SWCNT at the BHandH/STO-3G_{mag} level of theory). The corresponding difference for *armchair* (5, 5) SWCNT in Figure 7 is only 2.5 ppm.

According to ^{13}C NMR data in Table 4 and Figure 10 we can see that diatomics perturbs the electronic structure of the SWCNT significantly and thus it can be easily discriminate between addition at the rim (A1, Figure 10A) or in the middle of the tube (A2, Figure 10B). For example, addition at the rim in O_2 adducts makes an increase of ^{13}C isotropic shielding on attacked carbons of about 50 ppm (relative to pristine SWCNT), while in central part changes shieldings only by several ppms. Similarly, anisotropy changes significantly more during the rim addition (Δ = -104 ppm) than the central part addition (Δ = -40 ppm). In contrast, asymmetry parameter decreases during the rim addition (Δ = -0.4), while increase during the central part addition (Δ = 0.8). Figure 10 clearly shows a drop of carbon chemical shifts at the site of attachment. Besides, the neighboring carbons experience only very modest changes (up to 10 ppm). Interestingly, the magnitude of changes ("peak" intensities) depends on the type of diatomics. Similar plots in Figure S3 show the corresponding differences of individual carbon shielding anisotropies. In this case the magnitudes of observed "peaks" are about two times larger (about 180 ppm).

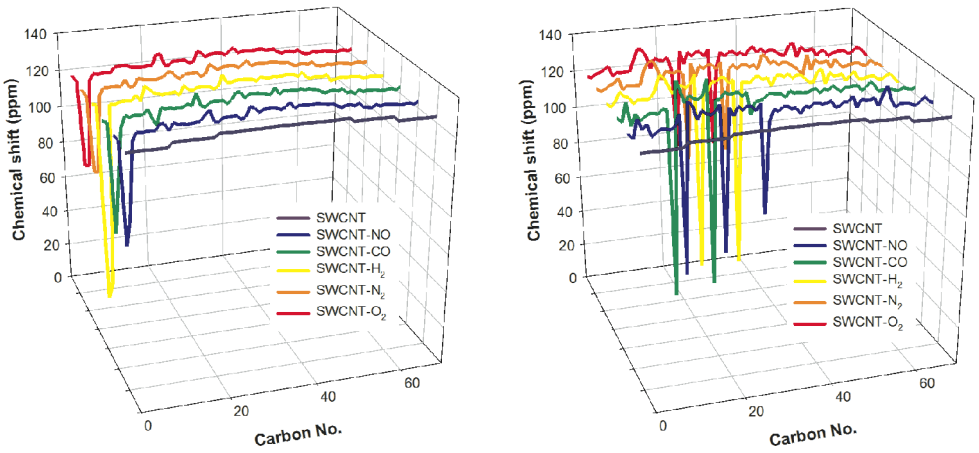

Figure 10. Calculated ^{13}C chemical shifts in pristine SWCNT and SWCNT-*AB* adducts. The diatomics addition was performed at position A1 (left) and position A2 (right) and calculated at the CAM-B3LYP/ STO-3G$_{mag}$ level of theory.

Addition of diatomics at A1 and A2 sites markedly changes the SWCNT peaks in the 1000 – 1700 cm^{-1} region. The signals in this region are more split and of lower intensity. Thus it is interesting whether the footprint of attached diatomics in IR/Raman spectra changes regarding the position of attachment. Spectral patterns for adducts with a diatomic at the A1 (rim) site are similar for all substituents. The A2 (central part) substitution produces less defined splitting of signals and is clearly distinguishable from the A1. The corresponding IR spectra (Figure S4) show significantly higher number of low intensity signals in the region around ~800 cm^{-1}. Addition of diatomics causes a splitting and intensity decrease of signals in this spectral fragment. We would like to mention that there are few subtle qualitative differences in this "fingerprint" region, which in principle could help to distinguish between addition at the rim and in the middle of the tube or even between perpendicular (A1) and longitudinal (A2) position of substituents, as seen from Figure 11. This observation is important since it allows getting a deeper insight about the topology of SWCNT functionalization at the atomic level. This kind of information is very difficult (if not impossible) to get from contemporary experiments.

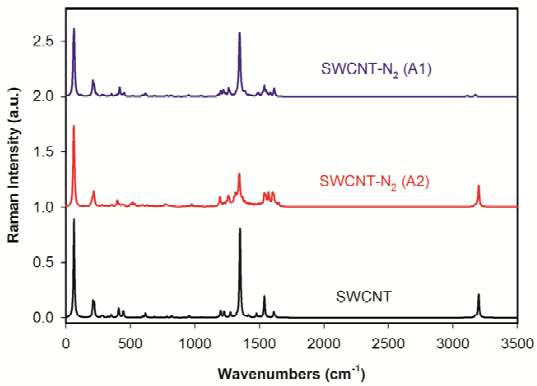

Figure 11. Comparison of the B3LYP/6-311G* calculated Raman spectra of *armchair* (5,5) SWCNT-N_2adduct with N_2 at position A1 or position A2. Spectrum of free pristine *armchair* (5, 5) SWCNT is shown for comparison.

5. Conclusions

We have presented a systematic computational study at the B3LYP/6-311G* level of theory on the impact of small diatomics addition (**O_2, N_2, H_2, NO and CO**) to two different sites at the side of model *armchair* (5, 5) SWCNT on the changes of CC bond lengths, HOMO/LUMO energies, the corresponding energy gap and NMR parameters of the gas molecules and individual carbon chemical shifts. The covalent bonding of diatomics decreased the CC bond order at the site of addition, decreased E_g by about 0.2 – 0.3 eV and caused huge changes in ^{13}C NMR chemical shifts (up to -100 ppm) and shielding anisotropies (up to about -180 ppm). Besides, it was possible to distinguish addition of particular diatomics, and gain some unique information about the functionalization site topology from the calculated Raman and IR spectra. The current theoretical study indicates the feasibility of an experimental verification of these NMR, IR and Raman predictions in the near future.

Acknowledgments

The National Center for Research and Development (projects No. PBS1/A5/15/2012 and GRAF-TECH/NCBR/10/29/2013) as well as the Faculty of Chemistry, University of Opole (Grant 8/WCH/2013-S) supported this work. The Grant Agency of the Czech Republic (P208/11/0105) and the Academy of Sciences of the Czech Republic (M200551205) are also acknowledged. Access to computing and storage facilities owned by parties and projects contributing to the National Grid Infrastructure Meta Centrum, provided under the programme "Projects of Large Infrastructure for Research, Development, and Innovations" (LM2010005), is greatly appreciated, as well as access to the CERIT-SC computing and storage facilities provided under the program Center CERIT Scientific Cloud, part of the Operational Program Research and Development for Innovations, reg. no. CZ. 1.05/3.2.00/08.0144.M. N. is a recipient of a Ph.D. fellowship from a project funded by the European Social Fund "Uniwersytecki Program Stypendialny 2011-2012" (POKL.08.02.01-16-002/11). The computer facilities in the Supercomputing and Networking Center ACK CYFRONET AGH in Krakow (grants MNiSW/SGI3700/ UOpolski/061/2008), and Wroclaw, as well as PL-Grid facilities at Zeus computer are also acknowledged.

Appendix A. Supplementary data

Supplementary material related to this article can be found, in the online version, at http://www.sciencedirect.com.

Figure Captions

Figure 1. The B3LYP/6-31G* optimized model of *armchair* (5, 5) SWCNT. A1 and A2 adsorption sites including C3, C4 and C22, C31 carbons are marked in blue. Two types of C-C bonds, tilted and perpendicular are marked off, too.

Figure 2. Different kinds of CC bonds in *armchair* (5, 5) SWCNT and their labeling are divided into (A) perpendicular and (B) tilted starting from one nanotube site to the opposite end. Adsorption sites (atoms C3, C4 and C22, C31) are marked as red (A1) and blue (A2) spots

Figure 3. Distribution of CC bond lengths in separate series of bonds (A) around the *armchair* (5, 5) surface (perpendicular to the axis) and (B) along the nanotube (tilted).

Figure 4. Distribution of CC bond lengths for pristine *armchair* (5, 5) SWCNT (blue marks) and with covalently bonded H_2 in position A1 (red open circles): (A) perpendicular to the nanotube axis and (B) tilted with respect to the nanotube axis.

Figure 5. Distribution of CC bond lengths for pristine *armchair* (5, 5) SWCNT (blue marks) and with covalently bonded H_2 in position A2 (red open circles): (A) perpendicular to the nanotube axis and (B) tilted with respect to the nanotube axis

Figure 6. HOMO-LUMO plots for *armchair* (5, 5) SWCNT (left panels) and (5, 5) SWCNT-H_2 adduct (right panels).

Figure 7. Distribution of individual carbon chemical shifts along the axis of *armchair* (5, 5) SWCNT. Experimental value for chiral (6, 5) SWCNT [38] is plotted (continuous green line) for comparison.

Figure 8. The B3LYP/6-311G* calculated Raman spectra of free *armchair* (5, 5) SWCNT and the studied SWCNT-*AB* adducts at position A1 (left) and position A2 (right).

Figure 9. Calculated (B3LYP/6-311G**) relative potential energy distribution (PED) of internal coordinates of *armchair* (5, 5) SWCNT. Only contributions of ν(CH) and ν(CC) stretching and δ(CCH) and δ(CCC) bending modes are displayed.

Figure 10. Calculated ^{13}C chemical shifts in pristine SWCNT and SWCNT-*AB* adducts. The diatomics addition was performed at position A1 (left) and position A2 (right) and calculated at the CAM-B3LYP/ STO-3G_{mag} level of theory.

Figure 11. Comparison of the B3LYP/6-311G* calculated Raman spectra of *armchair* (5, 5) SWCNT-N_2 adduct with N_2 at position A1 or position A2. Spectrum of free pristine *armchair* (5, 5) SWCNT is shown for comparison.

References

[1] Iijima, S. Helical microtubules of graphitic carbon. Nature. 1991, 354, 56-8.
[2] Kroto, H.W., Heath, J.R., O'Brien, S.C., Curl, R.F., Smalley, R.E. C60: Buckminsterfullerene. Nature. 1985, 318, 162 - 3.
[3] Novoselov, K.S., Geim, A.K., Morozov, S.V., Jiang, D., Zhang, Y., Dubonos, S.V., et al. Electric field in atomically thin carbon films. Science. 2004, 306, 666-9.
[4] Chełmecka, E., Pasterny, K., Kupka, T., Stobiński, L. Density functional theory studies of OH-modified open-ended single-wall zigzag carbon nanotubes (SWCNTs). J. Mol. Struct. (Theochem). 2010, 948, 93-8.
[5] Saloni, J., Kolodziejczyk, W., Roszak, S., Majumdar, D., Hill Jr., G., Leszczynski, J. Local and global electronic effects in single and double boron-doped carbon nanotubes. J. Phys. Chem. C. 2010, 114, 1528-33.
[6] Simon, P., Gogotsi, Y. Materials for electrochemical capacitors. Nature Materials. 2008, 7, 845-54.
[7] Dillon, A.C., Jones, K.M., Bekkedahl, T.A., Kiang, C.H., Bethune, D.S., Heben, M.J. Storage of hydrogen in single-walled carbon nanotubes. Nature 1997, 386, 377-9.
[8] Babaheydari, A.K., Jafari A., Moghadam G., Tavakoli K. Investigation and study of adsorption properties of H2S on carbon nanotube (8, 0) (SWCNT) using density functional theory calculation Advanced Science Letters. 2013, 19, 3201-5.
[9] Zettl, A. Extreme oxygen sensitivity of electronic properties of carbon nanotubes. Science. 2000, 286, 1801-4.
[10] Kong, J., Franklin, N.R., Zhou, C., Chapline, M.G., Peng, S., Cho, K., et al. Science. 2000, 287, 622-5.
[11] Peng, S., Cho, K.J. Chemical Control of Nanotube Electronics. Nanotechnology. 2000, 11, 57-60.
[12] Babanejad, S.A., Ashrafi, F., Ghasemi, A.S. Optimization of adsorption of oxygen gas on Carbon nanotubes surface,. Archives of Applied Science Research. 2010, 2 438 - 43.
[13] Ashrafi, F., Ghasemi, A.S., Babanejad, S.A., Rahimova, M. Optimization of Carbon Nanotubes for Nitrogen Gas Adsorption. J. of Appl.Sci. Eng. Tech. 2010, 2, 547-51.
[14] Ghasemi, A.S., Ashrafi, F., Babanejad, S.A., Rahimova, M. A Computational NMR Study of Chemisorption of Nitrogen-Doped on the surface of Single-Walled Carbon Nanotubes. Arch. Appl. Sc. Res. 2010, 2, 262.
[15] Foresman, J.B., Frisch, A. Exploring Chemistry with Electronic Structure Methods; Ed. Second ed. Pittsburg, PA, Gaussian Inc, 1996.
[16] Kar, T., Adkim, B., Duan, X., Pachter, R. Open-ended modified single-wall carbon nanotubes: A theoretical study of the effects of purification. Chem. Phys. Lett. 2006, 423, 126-30.
[17] Turabekova, M.A., Dinadayalane, T.C., Leszczynska, D., Leszczynski, J. Comprehensive Study on the Dissociative Chemisorption of NH3on the Sidewalls of Stone−Wales Defective Armchair J. Phys. Chem. C 2012, 116, 6012-21.
[18] Saremi, F., Haeri, H.H., Hasani, A.H., Mansouri, N. Adsorption of Carbon Monoxide on a (6, 6) Armchair Carbon Nanotube: Ab initio Study In: J. Phys.Theor. Chem., Islamic Azad University of Iran, 2008, 4, 235-8.
[19] Mansouri, N., Ghasemi, A.S., Aashrafi, F. Adsorption 17O, 15N and CO molecules on the surface of SWCNT: A Computational NMR study. Int. J. Chem.Tech Res. 2012, 4, 1295-301.
[20] Ghasemi, A.S., Rezaei, M., Molla, M. NMR Study of Gases Adsorption on Single-Walled Carbon Nano Tubes. Int. J.Chem Tech Res. 2013, 5, 1585-93.
[21] Zhao, J., Park, H., Han, J., Lu, J.P. Electronic Properties ofCarbon Nanotubes with Covalent Sidewall Functionalization. J. Phys.Chem. B 2004, 108, 4227−30.

[22] Liu, X., Sun, Y., Perez, L.A., Wen, W., Toney, M.F., Heeger, A.J., et al. Narrow-Band-Gap Conjugated Chromophores with Extended Molecular Lengths. J. Am. Chem. Soc. 2012, 134, 20609−12
[23] B. M. Maciejewska, M. Jasiurkowska-Delaporte, A. I. Vasylenko, Kozioł, K.K., Jurga, S. Experimental and theoretical studies on the mechanism for chemical oxidation of multiwalled carbon nanotubes. R. S. C. Adv. 2014, 4, 28826-28831.
[24] M.J. Duer, Blackwell Science Ltd., London,, ISBN: 9780632053513. Solid State NMR Spectroscopy: Principles and Applications. 2001.
[25] Mirzaei, M., Hadipour, N.L. An investigation of hydrogen-bonding effects on the nitrogen and hydrogen electric field gradient and chemical shielding tensors in the 9-methyladenine real crystalline structure: a density functional theory study. J. Phys. Chem. A,. 2006, 110, 4833-4838.
[26] Mintmire, J.W., Dunlap, B.I., White, C.T. Are fullerene tubules metallic? Phys. Rev. Lett. 1992, 68, 631-634.
[27] London, F. J. Phys. Radium (Paris). 1937, 8, 397-409.
[28] Ditchfield, R. Mol. Phys. 1974, 27, 789-807.
[29] Wolinski, K., Hilton, J.F., Pulay, P. Efficient implementation of the gauge-independent atomic orbital method for NMR chemical shift calculations. J. Am. Chem. Soc. 1990, 112, 8251-8260.
[30] Lim, S.H., Lin, J., Liu, L., Pan, H., Pan, H.L., Ji, W., et al. Functionalization Effect on the Electronic Properties of Single Walled Carbon Nanotubes. Funct. Mater. Lett. 2008, 1, 1−6.
[31] Andriotis, A.N., Menon, M., Srivastava, D., Froudakis, G. Extreme Hydrogen Sensitivity of the Transport Properties of SingleWall Carbon-Nantucket Capsules. Phys. Rev. B 2001, 64, 193401-1−-4.
[32] Gauss, J. Analytic second derivatives for the full coupled-cluster singles, doubles, and triples model: Nuclear magnetic shielding constants for BH, HF, CO, N2, N2O, and O3. J. Chem. Phys. 2002, 116, 4773-6.
[33] Zhiyong, Z., Steigerwald , M., Hybertsen , M., Brus , L., A., F.R. Electronic Structure of Tubular Aromatic Molecules Derived from the Metallic (5,5) Armchair Single Wall Carbon Nanotube. J. Am. Chem. Soc. 2004, 126, 3597-607.
[34] Mc Murry, J. Organic chemistry fourth edition. Warsaw, Brooks/Cole Publishing Company ITP An International Thomson Publishing Company, 2003.
[35] Stobiński, L., Peszke, J., Lin, H.-M. Rev. Adv. Matter Sci. 2003, 5, 363-70.
[36] Chełmecka, E., Pasterny, K., Kupka, T., Stobiński, L. DFT studies of OH-functionalized open-ended zigzag, arm-chair and chiral single wall carbon nanotubes. Phys. Status Solidi A. 2011, 208, 1774-7.
[37] Chełmecka, E., Pasterny, K., Kupka, T., Stobiński, L. DFT studies of COOH tip-functionalized zigzag and armchair single wall carbon nanotubes. J. Mol. Model. 2012, 18, 2241-6.
[38] Engtrakul, C., Davies, M.F., Mistry, K., Larsen, B.A., Dillon, A.C., Heben, M.J., et al. Solid-State ^{13}C NMR Assignment of Carbon Resonances on Metallic and Semiconducting Single-Walled Carbon Nanotubes. J. Amer. Chem. Soc. 2010, 132, 9956-7.
[39] Dresselhaus, M.S., Dresselhaus, G., Jorio, A. Raman spectroscopy of carbon nanotubes in 1997 and 2007. J. Phys. Chem. C. 2007, 111, 17887-93.
[40] R. Schönfelder, F. Avilés, A. Bachmatiuk, J.V. Cauich-Rodriguez, M. Knupfer, B. Büchner, et al. On the merits of Raman spectroscopy and thermogravimetri analysis to asses carbon nanotube structural modifications. Appl Phys A 2012, 106, 843-52.
[41] Saito, R., Dresselhaus, M.S., Dresselhaus, G. Physical Properties of Carbon Nanotubes. London, Imperial College Press, 1998.

[42] Frisch, M.J., G. W. Trucks, H. B. Schlegel, G. E. Scuseria, M. A. Robb, J. R. Cheeseman, et al. Gaussian 09, Revision A.02. Gaussian, Inc., Wallingford CT, 2009.
[43] Yanai, T., Tew, D., Handy, N. A new hybrid exchange-correlation functional using the Coulomb-attenuating method (CAM-B3LYP. Chem. Phys. Lett. 2004, 393 51-7.
[44] Voronkov, E., Rossikhin, V., Okovytyy, S., Shatckih, A., Bolshakov, V., Leszczynski, J. Novel physically adapted STO$^{\#\#}$-3G basis sets. Efficiency for prediction of second-order electric and magnetic properties of aromatic hydrocarbons. I. J. Quantum Chem. 2012, 112, 2444-9.
[45] Kaminský, J., Buděšínský, M., Taubert, S., Bouř, P., Straka, M. Fullerene C70 characterization by 13C NMR and the importance of the solvent and dynamics in spectral simulations. Phys. Chem. Chem. Phys. 2013, 15, 9223-30.
[46] Remya, K., Suresh, C.H. Which density functional is close to CCSD accuracy to describe geometry and interaction energy of small non-covalent dimers? A benchmark study using Gaussian09. J. Comp. Chem. 2013, 34, 1341-53.
[47] Buczek, A., Makowski, M., Jewgiński, M., Latajka, R., Kupka, T., Broda, M.A. Toward engineering efficient peptidomimetics. Screening conformational landscape of two modified dehydroaminoacids. Biopolymers. 2013, 101, 28-40.
[48] Radula-Janik, K., Kupka, T., Ejsmont, K., Daszkiewicz, Z., Sauer, S.P.A. Halogen effect on structure and 13C NMR chemical shift of 3,6-disubstituted-N-alkyl carbazoles. Magn. Reson. Chem. 2013, 51, 630-5.
[49] Kupka, T., Stachów, M., Chełmecka, E., Pasterny, K., Stobińska, M., Stobiński, L., et al. Efficient modeling of NMR parameters in carbon nanosystems. J. Chem. Theor. Comput. 2013, 9 4275–86.
[50] Kutzelnigg, W., Fleischer, U., Schindler, M. NMR Basic Principles and Progress. Springer-Verlag, Berlin, Heidelberg, 1990, 23, 165-262.
[51] Chesnut, D.B. The Ab Initio Computation of Nuclear Magnetic Resonance Chemical Shielding. New York, VCH Publishers, 1996.
[52] Kupka, T., Ruscic, B., Botto, R.E. "Hartree-Fock and Density Functional Complete Basis-Set (CBS) Predicted Nuclear Shielding Anisotropy and Shielding Tensor Components". Solid State Nucl. Magn. Reson. 2003, 2, 143-67.
[53] Kupka, T., Chełmecka, E., Pasterny, K., Stachów, M., Stobiński, L. DFT calculations of structures, 13C NMR chemical shifts and Raman RBM mode of simple models of small diameter (4.0) zigzag carboxylated single wall carbon nanotubes. Magn. Reson. Chem. 2012, 50, 142-51.
[54] R. Dennington, T. Keith, Millam, J. GaussView. Semichem Inc., Shawnee Mission, KS, 2009.
[55] Huber, K.P., Herzberg, G.H. Constants of Diatomic Molecules. New York, Van Nostrand-Reinhold, 1979.
[56] L.E. Sutton (Ed.) Tables of Interatomic Distances and Configuration in Molecules & Ions London, The Chemical Society, 1965.
[57] Wilson, E.B. J. Chem. Phys. 1939, 7, 1047−52.
[58] Wilson, E.B., Decius, J.C., Cross, P.C. Molecular vibrations. New York1980.
[59] Yamamoto, S., Kaminsky, J., Bour, P. Structure and vibrational motion of insulin from Raman optical activity spectra. P. Anal. Chem. . 2012, 84, 2440-51.
[60] Irle, S., Mews, A., Morokuma, K. Theoretical Study of Structure and Raman Spectra for Models of Carbon Nanotubes in Their Pristine and Oxidized Forms. J. Phys. Chem. A. 2002, 106, 11973-80.
[61] Kupka, T., Stachów, M., Stobiński, L., Kaminský, J. in preparation.